Sputter-induced crystalline layers and epitaxial overlayers on quasicrystal surfaces

2008 J. Phys.: Condens. Matter 20 314008

(http://iopscience.iop.org/0953-8984/20/31/314008)

IOP PUBLISHING JOURNAL OF PHYSICS: CONDENSED MATTER

J. Phys.: Condens. Matter **20** (2008) 314008 (11pp) doi:10.1088/0953-8984/20/31/314008

REVIEW ARTICLE

Sputter-induced crystalline layers and epitaxial overlayers on quasicrystal surfaces

M Shimoda[1] **and H R Sharma**[2]

[1] National Institute for Materials Science, 1-2-1, Sengen, Tsukuba, Ibaraki 305-0047, Japan
[2] Department of Physics, University of Liverpool, Liverpool L69 3BX, UK

E-mail: SHIMODA.Masahiko@nims.go.jp and H.R.Sharma@liv.ac.uk

Received 24 May 2008
Published 11 July 2008
Online at stacks.iop.org/JPhysCM/20/314008

Abstract

We present here an overview of surface and interface studies on various quasicrystals, focusing on areas where reflection high-energy electron diffraction plays an important role. Subjects included here are sputter-induced crystalline layers, surface alloying and epitaxial films. These phenomena are observed on the high symmetry surface of Al-based quasicrystals, such as decagonal Al–Ni–Co, icosahedral (i) Al–Cu–Fe and i-Al–Cu–Ru. For comparison, studies on i-Ag–In–Yb quasicrystal, an isostructure of the binary i-Cd–Yb quasicrystal, and ξ'-Al–Pd–Mn approximant are also included.

1. Introduction

Recent success in the synthesis of high quality quasicrystals as large single grains has opened up new fields in surface science, and a variety of studies on clean surfaces of quasicrystals and interfaces between quasiperiodic surfaces and overlayers have been reported [1–4]. A sputter-induced crystalline layer is a phenomenon that is commonly encountered during sample preparation of quasicrystals under ultra-high vacuum (UHV). For various Al-based quasicrystals, ion sputtering of quasicrystal surfaces induces depletion of Al [5, 6] and results in the formation of crystalline overlayers [7–16]. This crystalline overlayer can be re-quasicrystallized by annealing. Since sputtering and annealing are the requisite processes for producing clean and smooth surfaces, sputter-induced crystalline layers are an important issue in the surface study of quasicrystals.

Film growth, including epitaxy on quasicrystalline substrates, is another interesting subject. Epitaxy is normally regarded as a phenomenon in crystalline systems in which a crystalline film is grown on a crystalline substrate with a certain orientational correlation between the film and substrate. This definition of epitaxy can be extended naturally to quasiperiodic films and substrates: a crystalline or quasicrystalline film is grown on a crystalline or quasicrystalline substrate with a certain orientational correlation between the film and substrate.

One of the motivations for epitaxy study on quasicrystals is to evoke new phenomena by inducing quasiperiodic structure into various materials. Creating single-element quasicrystalline films is also of interest, since chemically simpler quasicrystalline systems provide better opportunities to unravel the secrets of quasicrystal formation. Epitaxy is also important for bulk systems where interfaces between quasicrystals and crystals are formed, because the mechanical or thermal properties of the system can be altered by the nature of interfaces. Quasicrystal–crystal interfaces in bulk systems are discussed in another paper [17].

In this contribution, we present an overview of surface studies on quasicrystals performed in our laboratory. Subjects presented here are sputter-induced crystalline layers and epitaxial overlayers on various quasicrystals including decagonal (d) Al–Ni–Co, icosahedral (i) Al–Cu–Fe, i-Al–Cu–Ru and i-Ag–In–Yb. Results on ξ'-Al–Pd–Mn, an approximant of i-Al–Pd–Mn, are also described. All the samples we used and information obtained on overlayers are listed in table 1.

One of the features of our studies is the successful use of reflection high-energy electron diffraction (RHEED), a

Table 1. List of samples. Methods to produce sputter-induced crystalline layers (section 3) and epitaxial layers (section 4) together with structures of these overlayers are shown. Abbreviations: In. = In surfactant, depo. = deposition, diff. = diffusion, bcc = body-centered cubic, sc = simple cubic.

Samples	Surface	Method	Structure	Domain
d-Al–Ni–Co	Tenfold	Sputter	bcc	Multiple
i-Al–Cu–Fe	Fivefold	Sputter	bcc	Multiple
i-Al–Cu–Ru	Fivefold	Sputter	bcc	Unknown
ξ'-Al–Pd–Mn	Pseudo-tenfold	Sputter	sc	Single
i-Ag–In–Yb	Fivefold	Sputter	Not ordered	—
d-Al–Ni–Co with In.	Tenfold	Au depo.	fcc	Multiple
d-Al–Ni–Co with In.	Tenfold	Au depo.	fcc	Multiple
d-Al–Ni–Co	Tenfold	Sn diff.	Quasiperiodic	—
i-Al–Cu–Fe	Fivefold	Bi depo.	Quasiperiodic + pseudo-sc	Multiple

powerful tool for surface study. RHEED patterns provide information on average surface structure, such as roughness, lattice parameters and the symmetry of surface reconstruction, over the macroscopic scale. In addition, RHEED as well as low-energy electron diffraction (LEED) gives us information about long-range order such as quasiperiodicity, which is an indispensable feature for quasicrystal study. Generally, both macroscopic measurements giving average structures and microscopic ones giving atomic scale images (like STM) are essential for understanding a certain surface and are used complementarily.

From an experimental point of view, one of the major advantages of this technique is the availability of *in situ* observation, which is realized by the unique geometrical arrangement employed in RHEED observations. A high-energy electron beam from an electron gun is directed at the sample surface at a grazing angle. The beam diffracted at the surface impinges on a phosphor screen which faces the gun. This arrangement provides a large working space in front of the sample surface and makes it possible to perform RHEED observations and various surface treatments, such as deposition, heating and ion sputtering, at the same time. This is the reason why RHEED is used not only for clean surfaces but also for epitaxy studies.

2. Experimental details

Samples were cut from large single-grain ingots perpendicular to the tenfold axis (for d-$Al_{72}Ni_{12}Co_{16}$ [18]), fivefold axis (i-$Al_{63}Cu_{23}Fe_{13}$ [19], i-$Al_{65.5}Cu_{19.5}Ru_{15}$ [20] and i-$Ag_{42}In_{42}Yb_{16}$ [21]), and the pseudo-tenfold axis (ξ'-$Al_{77.5}Pd_{19}Mn_{3.5}$ [22]), respectively, and then mechanically polished down to 0.25 μm using diamond paste. The samples were mounted on a molybdenum holder fixed with small tantalum pins and inserted into a UHV chamber (base pressure 1×10^{-8} Pa), equipped with a RHEED system (electron gun and phosphor screen), an ion gun for sputtering and a rotatable sample stage with a heating mechanism for the samples.

A clean surface was prepared by repeated cycles of Ar^+ ion sputtering (15–30 min 2–5 keV) and annealing up to ∼700 K (d-Al–Ni–Co), ∼770 K (i-Al–Cu–Fe), 1050–1200 K (i-Al–Cu–Ru), ∼620 K (i-Ag–In–Yb) and ∼950 K (ξ'-Al–Pd–Mn), respectively. Chemical composition change was monitored by XPS. An optical pyrometer (emissivity = 0.35) was used to measure the sample temperature. Note that the i-Al–Cu–Ru sample was not large enough to permit monitoring by the pyrometer. True temperature was estimated to be 100–150 K lower than indicated.

RHEED patterns were observed with an incident electron beam of 20–30 keV and a phosphor screen located at 200 mm from the sample center. Rotating the sample stage allows RHEED patterns to be observed along various azimuthal angles, provided the electron beam is not blocked by the sample-holding pins. For the small i-Al–Cu–Ru sample, this beam blocking happens over a wide range of angles.

Au depositions on the tenfold surface of d-Al–Ni–Co were performed at room temperature from a liquid-nitrogen-cooled evaporator with a tungsten basket. A quartz crystal oscillator was used as a thickness monitor. The deposition rate was 0.1–0.2 nm min^{-1}. After deposition, the sample was heated at a rate of 2 K min^{-1}. The chamber pressure was kept below 4×10^{-8} Pa during the evaporation and annealing. Pt was deposited in a similar way.

Bismuth depositions on the fivefold surface of i-Al–Cu–Fe were performed from a Knudsen cell at room temperature. The pressure was kept at a low 10^{-7} Pa during deposition. Flux calibration of the sources is achieved by measuring the coverage directly from the STM images at low coverage. The flux was cross-checked by calculating the thickness of a Bi thin film deposited on Pd(111) from the intensity of the photoemission core-level spectra. The estimated value is 3.4×10^{-2} ML s^{-1}.

A layer of Sn film was produced by means of surface diffusion as follows. The back side of the sample, which contacts with the sample holder, is partly coated in advance with a small amount of Sn. On heating the sample with a heating unit beneath the holder, the Sn on the back melts and starts to spread over the surface, resulting in a layer of Sn film. As seen in the case of Sn diffusion on the Al surface, we can expect the formation of a single layer due to Stranski–Krastanov growth [23].

3. Clean surface and sputter-induced crystalline layer

3.1. The tenfold surface of d-Al–Ni–Co

d-Al–Ni–Co has well-defined quasiperiodic planes which are stacked periodically along a unique tenfold axis. There are

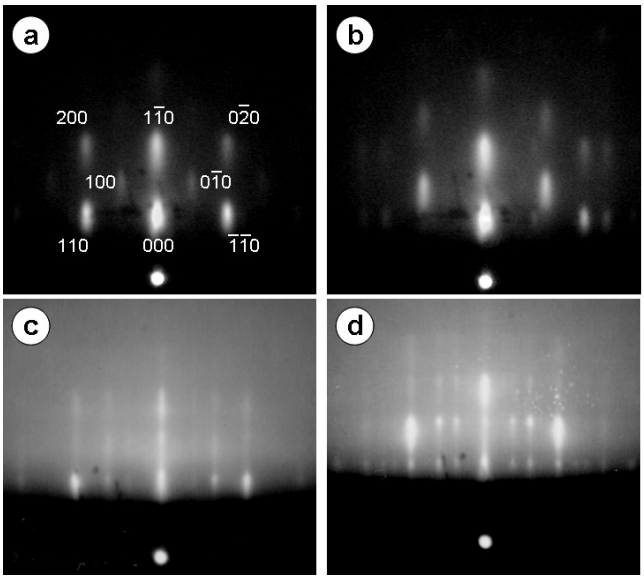

Figure 1. (a), (b) RHEED patterns from the sputtered tenfold surface of d-Al–Ni–Co observed with incident electron beam parallel to two kinds of the twofold axes. (c), (d) RHEED patterns after annealing observed along the same incident direction as in (a) and (b), respectively. (c) and (d) are reprinted from [16]. ©2000 Elsevier.

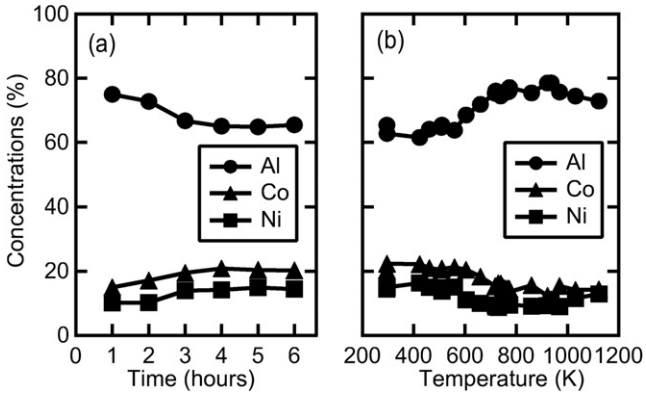

Figure 2. (a) Composition change of d-Al–Ni–Co during Ar^+ ion sputtering (1.5 keV). Due to preferential sputtering, the concentration of Al decreases with the passage of time. (b) Recovery of composition by annealing after Ar^+ ion sputtering. The concentration of each element is evaluated from the signal intensity of photoemission using the photoionization cross section and the elastic mean free path of electrons. Reprinted from [6]. ©2004 Elsevier.

two inequivalent sets of twofold axes, which are parallel to the quasiperiodic planes and perpendicular to the tenfold axis. Each set includes ten equivalents.

Typical RHEED patterns from the sputtered surface are shown in figures 1(a) and (b), which are observed with the incident electron beam along these two sets of twofold axes. These spotty patterns are likely to be due to diffraction from the crystalline islands on the surface and therefore suggest significant roughness, as predicted for a sputtered surface. Corresponding to the ten equivalent twofold axes, patterns similar to these two appear alternately every 18° for the rotation around the tenfold axis.

In accordance with previous studies on the irradiation effect [24–26, 16], these RHEED patterns are interpreted as diffractions from the (1$\bar{1}$0) surface of a cubic lattice: a pattern for the incident beam along the [001] direction (figure 1(a)) and a superposition of patterns along the [111] and [110] directions (figure 1(b)). The lattice constant is estimated to be ∼0.29 nm. As shown in figure 1(a), the spots that satisfy the relationship $h + k + l =$ odd are almost extinct, suggesting that the lattice has a bcc-like rather than a simple cubic structure. These RHEED patterns could be generated by a multiple twin structure: a layer of twin-related crystals which expose a certain plane as a surface and have different azimuthal orientations corresponding to the symmetry of the substrate. In the present case, the observed patterns can be explained by the multiple twin structure of bcc-like crystals which expose the (1$\bar{1}$0) planes and have azimuthal orientations corresponding to ten equivalent twofold axes. Since the angle between [111] and [110] is close to 36°, the superposition of patterns seen in figure 1(b) can be generated by diffractions from domains with different azimuthal orientation separated by 36° from each other.

After annealing at ∼700 K, these patterns are replaced with the more streaky patterns shown in figures 1(c) and (d), suggesting the formation of a smoother surface. Corresponding to the ten equivalent twofold axes, these patterns appear alternately every 18° during the rotation around the tenfold axis. This is consistent with the symmetry of the tenfold surface. Diffraction streaks are separated in a relation with the golden mean, $\tau(=(1+\sqrt{5})/2)$, the characteristic number frequently observed in quasiperiodic structures. This feature is consistent with quasiperiodicity. These facts indicate that the surface of d-Al–Ni–Co is quasiperiodic, as in the bulk.

The chemical composition of the surface was analyzed by XPS [6]. Figures 2(a) and (b) show the composition change during Ar^+ ion sputtering and the recovery of composition by annealing as a function of temperature. The surface after sputtering shows significant depletion of Al. The estimated chemical composition is about $Al_{65}Ni_{15}Co_{20}$ after sputtering and recovered to $Al_{75}Ni_{10}Co_{16}$ by annealing.

A number of other studies have been performed on the tenfold surfaces of d-Al–Ni–Co using various techniques such as LEED [27, 28], STM [29, 2] and ion scattering spectroscopy (ISS) [30, 31]. These studies show that the clean surface has the characteristic features of bulk truncation: no surface reconstruction is detected. This is consistent with RHEED observations.

3.2. The fivefold surface of i-Al–Cu–Fe

i-Al–Cu–Fe is a face-centered (F-type) icosahedral quasicrystal. The fivefold surfaces of i-Al–Cu–Fe and i-Al–Pd–Mn, an isostructure of i-Al–Cu–Fe, have been studied very extensively.

Figure 3 shows RHEED patterns from the sputtered surface observed at different azimuthal angles of the incident electron beam [32]. The spotty patterns suggest significant roughness of the sputtered surface. The triangular pattern seen in figure 3(a) can be interpreted as diffraction from a cubic lattice of the incident beam parallel to the [111] axis. The

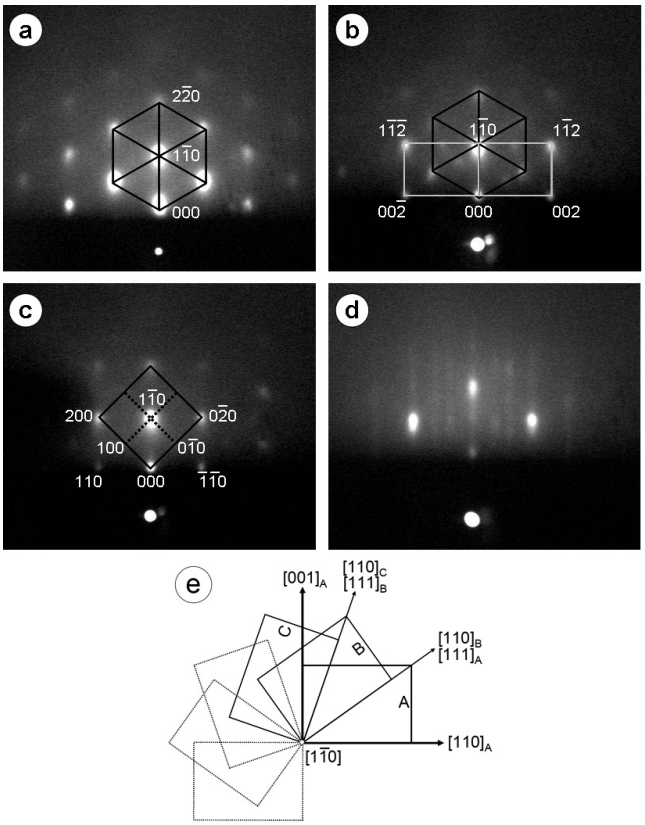

Figure 3. (a)–(c) RHEED patterns from the sputtered fivefold surface of i-Al–Cu–Fe observed along different azimuthal angles. These patterns are interpreted as diffractions from a cubic lattice for incident electron beam parallel to the (a) [111] axis, (b) [110] axis and (c) [001] axis, respectively. (d) RHEED pattern from a clean surface seen along the same incident direction for pattern (a). (e) A schematic view of the orientational relation in the multiple twin structure, e.g. $[111]_A$ (=the [111] axis of domain-A) is very close to the $[110]_B$, and so forth.

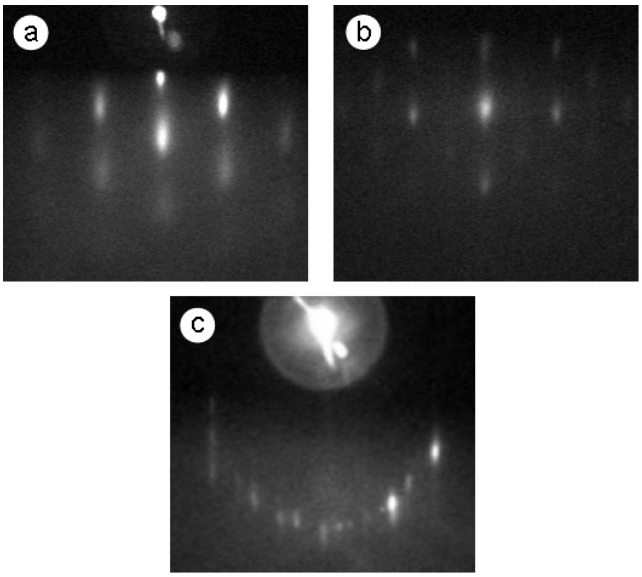

Figure 4. (a), (b) RHEED patterns from the sputtered fivefold surface of i-Al–Cu–Ru observed along different azimuthal angles. (c) RHEED pattern from the same sample after annealing. Figure (c) is reprinted from [33]. ©2005 Elsevier.

orientation of this triangular lattice indicates that the surface plane is parallel to the $(1\bar{1}0)$ plane ($(1\bar{1}0)$-oriented surface). Rotation of the sample by $\sim$36° around the z axis (= the fivefold axis of i-Al–Cu–Fe) produces the complex pattern seen in figure 3(b). This pattern can be interpreted as a mixture of two patterns, one expected for the incident beam along the [110] axis and the other along the [111] axis of the cubic lattice. The lattice constant is calculated to be 0.29–0.30 nm. Another 18° rotation around the z axis produces the square pattern as shown in figure 3(c), which is consistent with diffraction along the [001] axis of the same cubic lattice. It is clear from the indexing of the pattern that these spots satisfy the relationship $h + k + l =$ odd and are faint or extinct, suggesting that the lattice is more likely a bcc structure.

These features are explained by the multiple twin structure: a layer of twin-related cubic crystals exposing the $(1\bar{1}0)$-oriented surface with five different azimuthal orientations corresponding to the fivefold symmetry of the quasicrystalline substrate. The mixture of patterns seen in figure 3(b) is understood by the nature of this multiple twin structure: the [111] axis of one domain is very close to the [110] axis of another domain ($[111]_A$ and $[110]_B$ in figure 3(e)). The rotation angle of 18° corresponds to the angle between the [111] axis of one domain and the [001] axis of another (the angle between $[001]_A$ and $[111]_B$ in figure 3(e)).

In accordance with the multiple twin structure, a pattern observed at azimuthal angle θ often appears at $\theta + 36° \times n$ ($n =$ integer) upon rotating the sample around the z axis. However, these patterns are not completely identical to each other. For example, the pattern expected for the incident beam along the [111] axis is observed solely at one angle (figure 3(a)) and as a mixture of two patterns at another angle (figure 3(b)).

RHEED patterns from the annealed surface are totally different from those from the sputtered surface. As is the case with d-Al–Ni–Co, this is due to the regeneration of quasicrystalline order. Upon annealing, a streaked pattern begins to appear at 670 K. The pattern becomes clearer after a 1 h anneal at 770 K followed by an 800 K flash as shown in figure 3(d). This streaked pattern indicates the formation of a smooth surface. Analysis of the distance between streaks reveals long (L) and short (S) spacings of constant width. The width of these spacings is measured over several images and averaged, yielding an L/S ratio of 1.61 ± 0.04. This value is close to the golden mean, τ, suggesting that a clean surface with quasiperiodic structure is formed.

The chemical compositions estimated by XPS measurements are $Al_{50}Cu_{34}Fe_{16}$ for the sputtered surface and $Al_{64}Cu_{26}Fe_{10}$ after annealing at 770 K.

3.3. The fivefold surface of i-Al–Cu–Ru

i-Al–Cu–Ru is an isostructure of i-Al–Cu–Fe. Predictably, diffraction patterns observed from the sputtered fivefold surface are similar to those of i-Al–Cu–Fe, as shown in figures 4(a) and (b) [33]. The triangular pattern seen in figure 4(a) is interpreted as diffraction from a cubic lattice

with an exposed $(1\bar{1}0)$-oriented surface to the incident electron beam parallel to the [111] axis. Rotation of the sample by ∼54° around the z axis produces the pattern shown in figure 4(b), which is recognized as a pattern from the same cubic lattice for the incident beam along the [001] axis. However, spots like $h + k + l =$ odd are almost extinct, indicating that the lattice is more likely a bcc. The lattice constant calculated from these patterns is ∼0.31 nm. Since no other RHEED patterns were obtained due to the small sample, the multiple twin structure, as seen in the case of i-Al–Cu–Fe, could not be confirmed.

The surface phase transition to the quasiperiodic structure is observed at ∼900 K, where diffraction streaks with τ-related separation appear (figure 4(c)). To obtain a smooth surface with a step-terrace structure, subsequent heating up to 1050–1200 K is required.

3.4. The pseudo-tenfold surface of ξ'-Al–Pd–Mn

The ξ'-Al–Pd–Mn, an approximant of i-Al–Pd–Mn, is an orthorhombic crystal with lattice constants $a_{\xi'} = 2.389$ nm, $b_{\xi'} = 1.656$ nm and $c_{\xi'} = 1.256$ nm [34]. Along the $b_{\xi'}$ axis (the pseudo-tenfold axis), four different types of layers are stacked at $y = 0$, 0.12, 0.16 and 0.25 in units of $b_{\xi'}$. The rest of the layers in the unit cell can be obtained by symmetry operations.

RHEED patterns from the sputtered surface are shown in figures 5(a)–(f) [35]. These patterns were obtained at different azimuthal angles by rotating the sample around the surface normal, the $b_{\xi'}$ axis. The spotty patterns suggest significant roughness of the sputtered surface. The triangular and rectangular patterns shown in figures 5(a) and (e) are explained by diffraction from a cubic lattice with its $(1\bar{1}0)$-oriented surface plane for the incident beam along the [111] and [110] axes, respectively. The estimated lattice constant of the cubic lattice is ∼0.30 nm. The diffraction patterns presented in figures 5(b)–(d) appear at 20°, 33°, 114° and −20° rotations from the position of the triangular pattern. The measured rotation angles are very close to the angles of the [112], [113], $[\bar{1}\bar{1}1]$ and [331] axes from the [111] axis of a cubic lattice, respectively, as shown in figure 5(g). Predictably, these diffraction patterns are consistent with diffraction from the same cubic lattice with the $(1\bar{1}0)$-oriented surface plane for the incident beam along the [112], [113], $[\bar{1}\bar{1}1]$ and [331] axes, respectively. The indexing of the RHEED pattern for [110] incidence is illustrated in figure 5(e). Unlike the sputtered surfaces of quasicrystals described above, this surface shows no extinction of diffraction spots, suggesting the formation of a simple cubic lattice such as a CsCl-type structure. In addition, the RHEED patterns show no trace of multiple twin structures such as superposition of two diffraction patterns.

The chemical composition of the sputtered surface is estimated to be $Al_{63}Pd_{35}Mn_2$. The obtained composition shows depletion of Al in the surface region, which is due to the preferential sputtering of Al as in the case of Al-based quasicrystals.

Upon annealing, diffraction spots become faint and vertical streaks start to appear at around 620 K. After annealing at 820 K, the pattern presented in figure 5(e) is replaced by a streaked pattern with brighter spots on circles, which is a typical feature of RHEED patterns from a smooth surface. This pattern consists of weak and strong streaks that yield a periodic spacing. The lattice parameter estimated from the distance between the nearest streaks is about 1.2 nm, which is close to the bulk lattice constant $c_{\xi'} = 1.256$ nm. The incident beam direction of this pattern is hence identified as parallel to the $a_{\xi'}$ axis, revealing that the sputter-induced layer is formed with the [110] axis oriented parallel to the $a_{\xi'}$ axis of the underlying bulk.

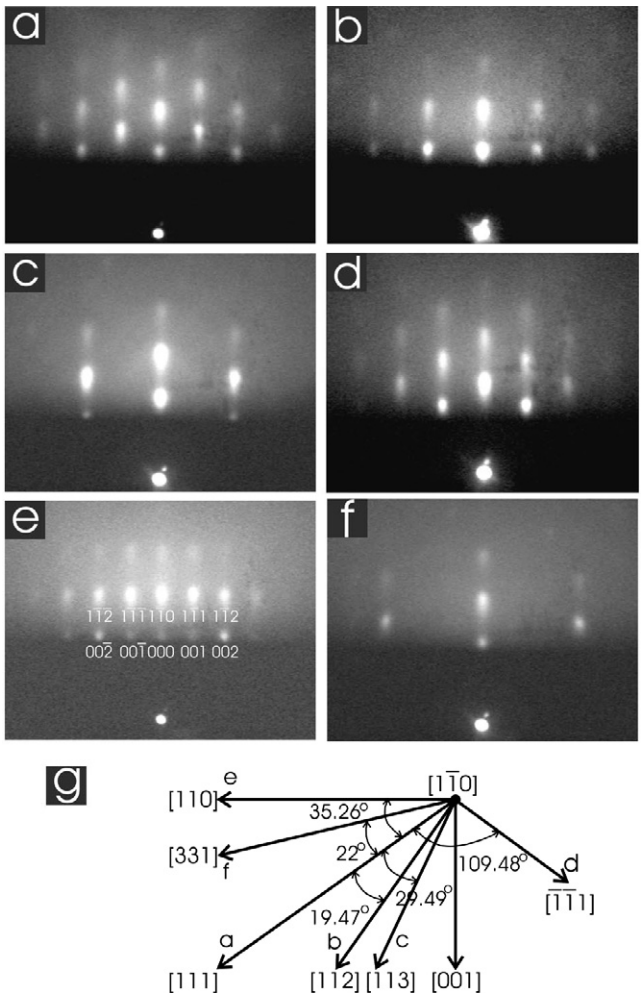

Figure 5. (a)–(f) RHEED patterns of the sputtered pseudo-tenfold surface of the ξ'-Al–Pd–Mn approximant observed along different azimuthal angles. Indexing of the pattern for [110] incidence is given in (e). (g) The relation between the azimuthal angles and axes of a cubic lattice. The angles given are the exact angles between the axes; measurement angles are given in the text. Reprinted from [35]. ©2005 The American Physical Society.

3.5. The fivefold surface of i-Ag–In–Yb

i-Ag–In–Yb is an isostructure of i-Cd–Yb [36], the first ever thermally stable binary quasicrystal. The lattice has a primitive icosahedral structure (P-type), in contrast to most Al-based icosahedral (F-type) quasicrystals. Although i-Cd–Yb is a focus of considerable interest because of its simplicity, the high

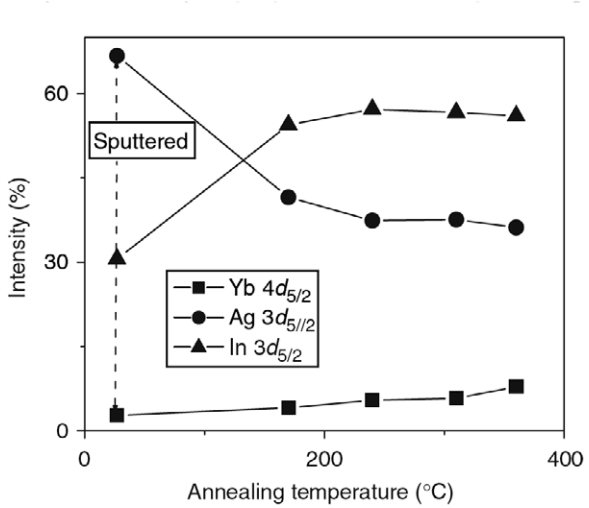

Figure 6. The intensity of Ag $3d_{5/2}$, In $3d_{5/2}$ and Yb $4d_{5/2}$ core-level photoemission from the fivefold i-Ag–In–Yb surface after sputtering (marked by a dotted line) and annealing at different temperatures. Reprinted from [37]. ©2007 Taylor and Francis.

vapor pressure of Cd impedes surface studies in UHV. Instead, i-Ag–In–Yb is derived from i-Cd–Yb by replacing Cd with Ag and In [21]. i-Ag–In–Yb is stable under vacuum, affording a unique opportunity to study P-type quasicrystal surfaces.

Since no recipe for the surface preparation of i-Ag–In–Yb was known, the chemical composition change caused by sputtering and annealing was studied before beginning other experiments [37]. Figure 6 shows the intensity of Ag $3d_{5/2}$, In $3d_{5/2}$ and Yb $4d_{5/2}$ core-level photoemission from the surface after sputtering and annealing at different temperatures. The surface after sputtering shows depletion of In and Yb. The chemical composition is estimated to be about $Ag_{71}In_{24}Yb_5$. Interestingly, In and Yb, which are preferentially sputtered, are heavier than Ag. This is exactly the opposite result to that seen in Al-based quasicrystals, where Al, the lightest element in the quasicrystal, is preferentially sputtered.

Upon annealing, the intensity of In and Yb is regained at around 470 K. For temperatures from 470 to 620 K, the intensity of all three elements remains unchanged. The chemical composition of the surface annealed at these temperatures is $Ag_{40}In_{45}Yb_{15}$, which is close to the bulk composition. The slight shift from the bulk composition may be attributed to artifacts in the evaluation of photoemission intensity.

In contrast to the Al-based quasicrystals, the sputtered fivefold surface of i-Ag–In–Yb does not show any well-defined diffraction spots. Instead, concentric rings of very weak intensity appear (figure 7(a)). The patterns remain unchanged with the rotation of the sample around the surface normal. Such patterns suggest that the surface after sputtering is not well ordered.

Upon annealing, diffraction patterns with streaks appear at 470 K (figure 7(b)). This feature does not change after further annealing up to 620 K, in accordance with the constant chemical composition in this temperature range. The streaks are spaced at τ-scaling distances, showing the quasicrystalline

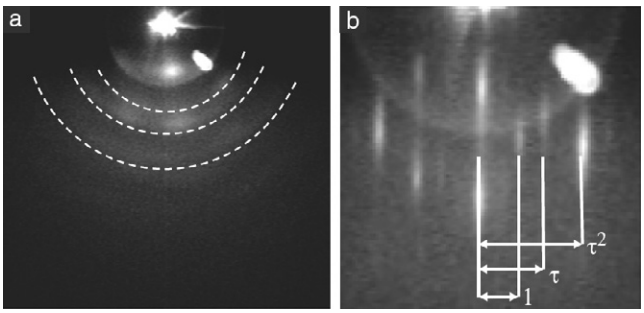

Figure 7. RHEED patterns from the fivefold i-Ag–In–Yb surface. (a) After sputtering and (b) after annealing at 470 K, showing τ-scaling diffraction streaks. Reprinted from [37]. ©2007 Taylor and Francis.

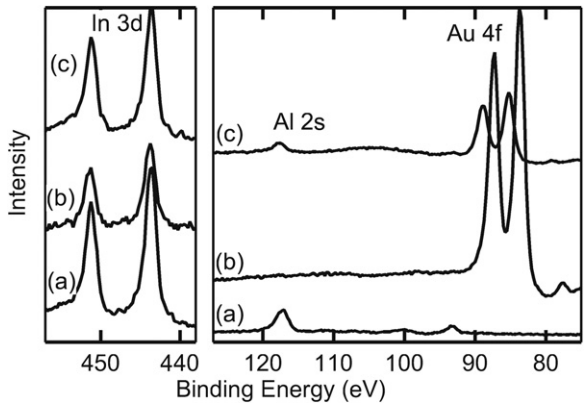

Figure 8. XPS spectra of In 3d, Al 2s and Au 4f emissions from the Au overlayer on an In-precovered tenfold surface of d-Al–Ni–Co, (a) before Au deposition (= after annealing to restore the quasicrystalline surface), (b) after the deposition of ∼10 ML Au, and (c) after Au deposition and subsequent annealing at 350–400 K. Reprinted from [6]. ©2004 Elsevier.

order of the surface. Equivalent diffraction patterns are observed when the sample is rotated azimuthally by 36°. This further suggests the quasicrystalline symmetry of the surface.

4. Epitaxial overlayers

4.1. Au on the tenfold surface of d-Al–Ni–Co with In surfactant

Initially, an In-precovered surface is prepared on the tenfold surface of d-Al–Ni–Co using surface diffusion [6, 38]. The thickness of the In layer is estimated to be 0.6 ML by XPS analysis. Au is deposited onto this In-precovered surface. The Au overlayer is thick enough for no XPS signals from the d-Al–Ni–Co substrate to be detected. The signal intensity of In 3d core-level photoemission does not change significantly even after Au deposition (spectra (a) and (b) in figure 8), suggesting that most of the In remains at the topmost surface even during Au deposition. This is consistent with the difference of the surface energy of stable planes between In and Au; In(001) has much lower surface energy than Au(111) [39].

With increasing temperature, the photoemission signal from Al emerges at 350–400 K, whereas no signals from Ni

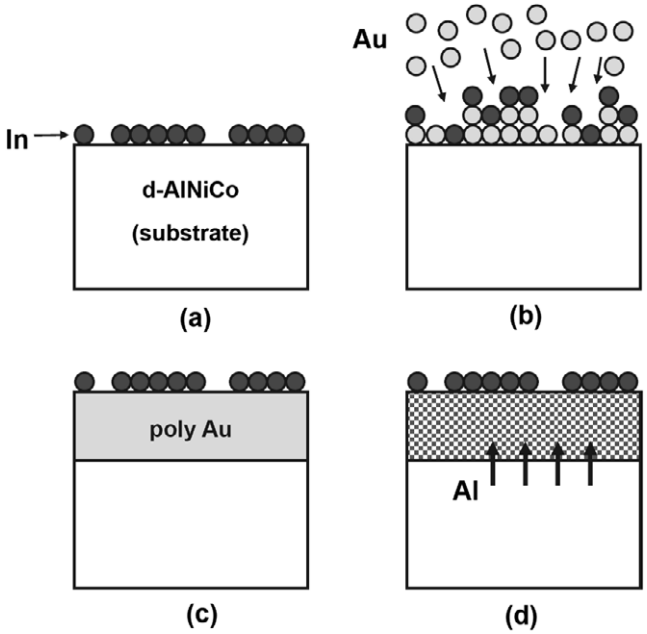

Figure 9. A model process deduced from XPS measurements for the formation of an Au–Al alloy layer on the In-precovered tenfold surface of d-Al–Ni–Co. (a) An In layer appeared after annealing to restore the quasicrystalline structure. (b) Indium atoms remain at the topmost surface, even during Au deposition. (c) An Au polycrystalline layer covered by an In layer was formed. (d) By heating the sample up to 300–400 K, a crystalline layer of Au–Al alloy was formed. Reprinted from [6]. ©2004 Elsevier.

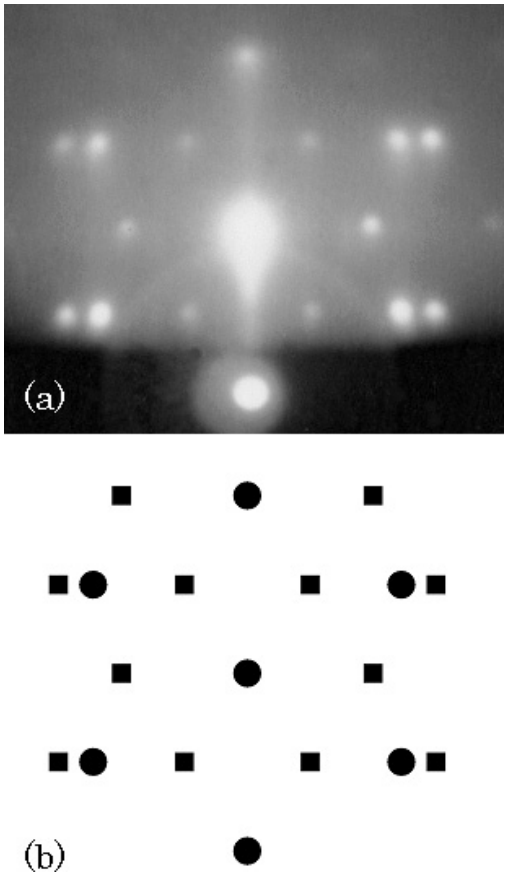

Figure 10. (a) RHEED pattern from the Au overlayer on the In-precovered tenfold surface of d-Al–Ni–Co after annealing. The direction of the incident electron beam is parallel to one of the twofold axes. (b) Schematic pattern of diffraction spots from an fcc(110) plane for the incident electron beam along the [001] direction (filled circles) and the [112] direction (filled squares). Reprinted from [38]. ©2001 Elsevier.

or Co are detected. In addition, the Au 4f peaks decrease in intensity and show a chemical shift of ∼1.7 eV (spectrum (c) in figure 8). This suggests that only Al atoms diffuse into the Au overlayer and that an Au–Al alloy is created (figures 9(a)–(d)). The average composition of the overlayer is estimated to be Au:Al ∼ 1:2.

The RHEED pattern from this surface is shown in figure 10(a), which is observed with the incident electron beam along one of the twofold axes of the substrate. Corresponding to the ten equivalent twofold axes, equivalent patterns are observed every 36° with respect to the rotation around the tenfold axis. This diffraction pattern is interpreted as the superposition of two patterns: one is predicted from the $(1\bar{1}0)$ plane of an fcc crystal for the incident electron beam along the [001] direction and the other is from the same crystal for the incident beam along the [112] direction (figure 10(b)). Since the angle between [001] and [112] is very close to 36°, this superposition could be generated by the multiple twin structure of fcc crystals—a layer of twin-related fcc crystals exposing the $(1\bar{1}0)$-oriented surface with ten different azimuthal orientations corresponding to the tenfold symmetry of the substrate. The lattice constant estimated from these patterns is ∼0.6 nm [38].

According to the definition given in the introduction, the overlayer of Au–Al alloy with the multiple twin structure is an epitaxial crystalline film grown on a quasicrystalline substrate, since the orientational correlation between the overlayer and the tenfold surface of d-Al–Ni–Co is apparent.

4.2. Pt on the tenfold surface of d-Al–Ni–Co with In surfactant

A similar result is obtained for Pt deposition on the same surface. After annealing, a chemical shift of ∼1.1 eV for Pt 3d photoemission peaks is observed [40]. The average composition of the overlayer is estimated to be Pt:Al ∼ 1:2.5.

Two kinds of RHEED patterns expected for diffractions from the $(1\bar{1}0)$ plane of an fcc crystal appear alternately every 18° during azimuthal rotation (figure 11) [40, 41]. The formation of an epitaxial overlayer of Pt–Al alloy with a multiple twin structure is thus confirmed.

4.3. Sn on the tenfold surface of d-Al–Ni–Co

Figure 12(a) shows the RHEED pattern from a layer of Sn film created by surface diffusion on the tenfold surface of d-Al–Ni–Co [42]. Since the diffraction spots are broad and streaky, it appears that the surface consists of finite two-dimensional regions such as step-terrace structures. The distances among the diffraction lines are related by τ with each other, suggesting quasiperiodic structure.

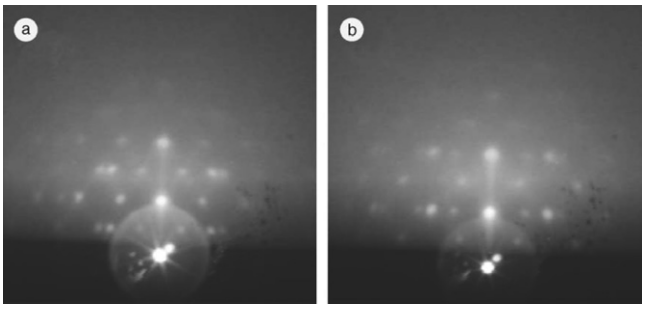

Figure 11. RHEED patterns from the Pt overlayer on the In-predeposited tenfold surface of d-Al–Ni–Co after annealing at 490 K. These two patterns are observed alternately every 18° for the rotation around the tenfold axis corresponding to two sets of twofold axes. Reprinted from [42]. ©2002 Elsevier.

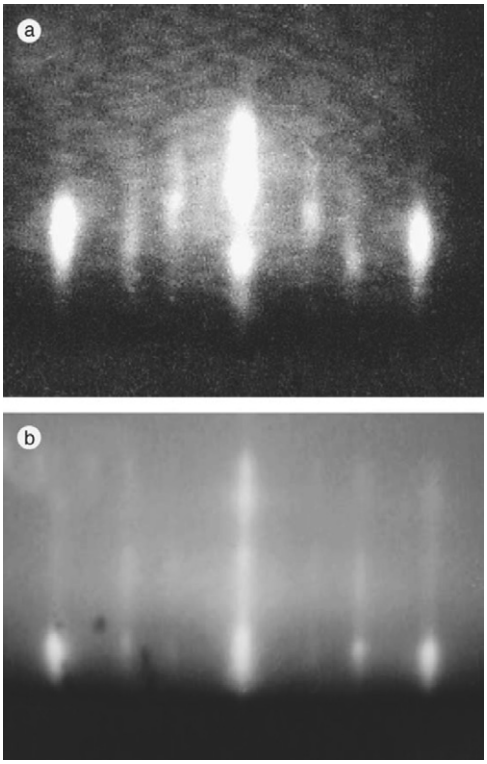

Figure 12. RHEED patterns from (a) the Sn-deposited tenfold surface of d-Al–Ni–Co after annealing and (b) the clean tenfold surface of d-Al–Ni–Co. Reprinted from [44]. ©2004 Elsevier.

4.4. Bi on the fivefold surface of i-Al–Cu–Fe

In the case of Bi deposition on the fivefold surface of i-Al–Cu–Fe, a wetting layer is formed first, followed by the growth of Bi islands for larger coverage [43]. An astonishing feature of this system is that, for multilayer coverage, Bi deposition yields islands with specific heights (magic height) corresponding to the stacking of a specific number of atomic layers. STM measurements have revealed that the height of the islands measured from the wetting layer is 1.3 nm or a multiple of this height. The vast majority of the islands are 1.3 nm high, which corresponds to the stacking of four atomic layers, considering the fact that the interlayer spacing along the pseudo-cubic [001] direction of the bulk Bi is 0.328 nm. This unusual growth morphology is interpreted as a quantum size effect and is explained by confinement of electrons within the film [43].

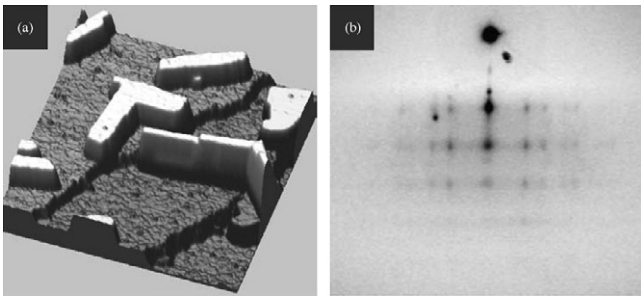

Figure 13. (a) STM image of the fivefold surface of i-Al–Cu–Fe after deposition of 4.5 ML of Bi. (b) RHEED image from the same surface. (a) is reprinted from [4]. ©2007 Taylor and Francis. (b) is reprinted from [45]. ©2005 The American Physical Society.

A typical RHEED pattern from the Bi islands is shown in figure 13(b). The pattern consists of diffraction spots aligned along straight lines, indicating transmission reflection diffraction through the 3D Bi islands. The small spots' size also demonstrates the good crystallinity of the islands. The patterns are consistent with those of a pseudo-cubic structure with a (001)-oriented surface. It should be noted that, although the exact crystal structure of Bi is trigonal, it can be regarded as a slightly distorted simple cube. The pseudo-cubic [001] corresponds to the trigonal $[01\bar{1}2]$ and the $(01\bar{1}2)$ plane is the closest packed one of the Bi crystal.

Comparison of the RHEED patterns from the Bi-deposited surface with those from the clean surface reveals that the Bi islands are aligned along the high symmetry directions of the substrate. Accordingly, the same diffraction pattern appears every 72° when the sample is rotated azimuthally. This demonstrates that Bi islands form a multiple twin structure with an epitaxial relationship between the islands and the substrate.

5. Discussion

The formation of sputter-induced crystalline layers is a common phenomenon in Al-based quasicrystals and approximants. In the case of the sputtered tenfold surface of d-Al–Ni–Co, RHEED reveals that a crystalline layer of a cubic lattice with a lattice constant of 0.29 nm is formed. The lattice constant is close to 0.2848 and 0.2863 nm for CsCl-type AlCo and AlNi [44], respectively, suggesting that a layer of β-phase $Al(Co_{1-x}Ni_x)$ alloy is formed. The faint spots of $h + k + l =$ odd indicate that the crystalline layer has a bcc-like rather than a simple cubic structure such as a genuine CsCl structure. It is highly likely that a chemical disorder between body-center and corner sites occurs and that these sites are occupied randomly by Al and transition metals. The Al-rich composition ($Al_{65}Ni_{15}Co_{20}$) even after the preferential sputtering might be a cause of this chemical disorder.

Almost the same conclusion applies to the sputtered fivefold surface of i-Al–Cu–Fe. The observed lattice constant 0.29–0.30 nm is very close to 0.290 76 nm for CsCl-type

AlFe [44]. Although no CsCl-type AlCu is known, the β-phase $Al(Cu_{1-x}Fe_x)$ alloy exists for a wide range of x values. Thus, it is concluded that a layer of $Al(Cu_{1-x}Fe_x)$ alloy with a multiple twin structure is formed [13, 14]. The faint but not extinct spots of $h + k + l =$ odd indicate that the lattice is neither a simple cubic nor a bcc, which is consistent with the formation of the β-phase $Al(Cu_{1-x}Fe_x)$ alloy with a chemical disorder between body-center and corner sites.

As described in section 3.2, diffraction patterns observed at azimuthal angles $\theta + 36^\circ \times n$ are similar but not completely identical to each other. This is partly due to an inhomogeneous distribution of domains with different azimuthal orientations. Since the position of the surface impinged by electron beams is moved by rotating the sample, the domains responsible for the diffraction would change depending on the azimuthal angles. It is also possible that anisotropic sputtering induces a preferential orientation to domains as previously reported [9].

RHEED patterns from the sputtered surface of i-Al–Cu–Ru exhibit diffraction of a type predicted for a cubic lattice. The estimated lattice constant, 0.31 nm, is consistent with 0.3036 nm for CsCl-type AlRu [44]. Although no other independent diffraction patterns are observed for this sample, it is highly likely that the sputtering induces the formation of a layer of alloy like $Al(Cu_{1-x}Ru_x)$.

In the case of the pseudo-tenfold surface of ξ'-Al–Pd–Mn, RHEED patterns from the sputtered surface reveal that a crystalline overlayer with a cubic lattice is formed. Unlike the case of the quasicrystals mentioned above, diffraction patterns exhibit no extinction of spots. This means that the sputter-induced crystalline layer has a simple cubic lattice like the CsCl structure rather than a bcc lattice. The estimated lattice constant $a \sim 0.30$ nm is close to 0.304 nm for CsCl-type AlPd [44]. Since the phase diagram of Al–Pd–Mn contains CsCl-type Al–Pd phases on the Al-poor side [45], sputtering of this surface would cause depletion of Al and then induce a composition shift towards the CsCl-type phases.

Another characteristic feature of this surface is that the crystalline layer has a single-domain structure rather than the multiple twin structure observed on the quasicrystal surfaces. This can be explained by lattice matching between the ξ'-Al–Pd–Mn substrate and the sputter-induced crystalline layers. RHEED measurements reveal that the [001] and [110] axes of the crystalline overlayer are oriented along the $c_{\xi'}$ and $a_{\xi'}$ axes of the bulk, respectively. The lattice parameters of the overlayer crystal along these axes are a and $a\sqrt{2}$, which are close to $c_{\xi'}/4$ and $a_{\xi'}/6$, respectively. Along the $a_{\xi'}$ axis, the lattice mismatch is about 7% with respect to the lattice constant of AlPd, while the mismatch is about 3% along the $c_{\xi'}$ axis. Because of this relatively small lattice mismatch, an epitaxial film of Al–Pd alloy can be formed commensurately, and hence it is likely that the overlayer grow as a single domain instead of a multiple twin structure. Due to this commensurate nature, the crystalline overlayer is likely to be stable by maintenance of the chemical order over a long range. Thus, this lattice-matching model can also explain the creation of the simple cubic crystalline layer.

In contrast to the case of Al-based quasicrystals, sputtering yields no crystalline overlayer on the fivefold surface of i-Ag–In–Yb. It is not unusual for well-ordered structures such as crystalline and quasicrystalline structures to be destroyed by ion sputtering without forming any other ordered structure. Therefore, the question is why sputter-induced crystalline layers are produced on the surface of particular quasicrystals and approximants.

In the case of the ξ'-Al–Pd–Mn approximant, the lattice-matching model can explain the creation of the crystalline overlayer as mentioned above. Obviously, this form of lattice matching never happens on a macroscopic scale on quasicrystal surfaces due to quasiperiodicity. However, lattice matching can be realized locally, and hence the multiple twin structure is created as an ensemble of crystals, each of which satisfies the lattice matching locally. In previous reports, a local lattice matching at the interfaces between AlNi (or AlCo) crystals and the tenfold surface of d-Al–Ni–Co [16] and between AlPd crystals and the fivefold surface of i-Al–Pd–Mn [46] are discussed.

Instead of these real-space analyses, methods based on the reciprocal space have been developed [47–49]. In the reciprocal space, lattice matching can be described without specifying atom positions explicitly, which provides a quantitative way for evaluating lattice matching. Details are described in other papers in this issue [50, 51]. For the case of sputter-induced crystalline layers, Widjaja *et al* discussed energetics by considering a coincidence of reciprocal lattice planes and successfully explained the orientational relationships between the overlayers and quasicrystalline substrates including the tenfold surface of d-Al–Ni–Co and the fivefold surface of i-Al–Cu–Fe [48].

Deposition is a common method used to create films on various surfaces. With the aid of In as a surfactant, Au deposition on the tenfold surface of d-Al–Ni–Co and subsequent annealing produces a crystalline layer of Au–Al alloy with the multiple twin structure. The estimated lattice constant ~0.6 nm is much larger than 0.408 nm for the fcc Au and very close to 0.5998 nm for the CaF_2-type $AuAl_2$ [44]. In addition, the surface composition estimated by XPS is close to $AuAl_2$. Thus, it is concluded that an epitaxial crystalline layer of $AuAl_2$ is formed. The same discussion is true for Pt deposition on the same surface, where the crystalline layer consists of CaF_2-type $PtAl_2$ with a lattice constant of 0.5922 nm [44]. The chemical shift of Au 4f and Pt 3d photoemission peaks (~1.7 eV and ~1.1 eV, respectively) gives more evidence of surface alloying. The formation of $AuAl_2$ crystals with the multiple twin structure is also confirmed by XPD measurements [38].

Interestingly, Al sites in the $AuAl_2$ (or $PtAl_2$) crystal make up a cubic sublattice with a lattice constant of 0.2999 nm (0.2961 nm), half of the crystal lattice constant. This value is very close to the Al–Al bond length of CsCl-type AlNi or AlCo crystal (= the lattice constant of these crystals), and therefore local lattice matching can explain the formation of $AuAl_2$ ($PtAl_2$) crystals with a multiple twin structure.

The numerical analysis in the reciprocal lattice demonstrates that the observed orientational relationship between the epitaxial crystalline layer of $AuAl_2$ ($PtAl_2$) and the tenfold surface of d-Al–Ni–Co is energetically preferable [48]. An similar method was applied to explain the orientation of AsAl islands

formed on the tenfold surface of d-Al–Ni–Co, where a matching of reciprocal lattice points is considered [47].

Generally, surfactants suppress the formation of 3D islands by reducing the diffusivity of deposited atoms and promote layer-by-layer growth, as observed in the homoepitaxial growth of Cu(111) [52]. In the present case, however, the epitaxial layer induced is not an Au (Pt) film but an $AuAl_2$ ($PtAl_2$) film. This means that In not only promotes layer-by-layer growth but also enhances the migration of Al into the Au (Pt) overlayer.

In the case of elements with low surface energy such as Sn (0.611 J m^{-2} for Sn(001)) and Bi (0.537 J m^{-2} for Bi(100)) [39], the overlayer on quasiperiodic surfaces exhibits a different morphology. Sn on the tenfold surface of d-Al–Ni–Co forms a single atomic layer (a wetting layer) with a quasiperiodic structure for monolayer coverage. According to the definition, this pseudomorphic film is also an epitaxial film. The same result is confirmed in the STM study of Sn deposition on the fivefold surface of i-Al–Cu–Fe [53]. Multilayer coverage is also studied on the i-Al–Cu–Fe surface and reveals the growth mode to be a Stranski–Krastanov type (layer plus island growth) [54]. The details of this multilayer film are not clarified yet.

Similar to the case of Sn, Bi deposition on the fivefold surface of i-Al–Cu–Fe produces a wetting layer with a quasiperiodic structure. It should be noted that the quasiperiodic structure of the Bi wetting layer is demonstrated by LEED and helium atom scattering (HAS) for Bi deposition on the fivefold surface of i-Al–Pd–Mn [55].

After completing the wetting layer, Bi grows as islands of 'magic height'. RHEED patterns reveal that these islands have a periodic structure with a trigonal $(01\bar{1}2)$ surface plane and five different orientations. This is another example of the multiple twin structure. Preferential matching between the fivefold plane of i-Al–Cu–Fe and the $(01\bar{1}2)$ plane of Bi is demonstrated in a bulk composite system where Bi particles are embedded into an i-Al–Cu–Fe matrix [17].

Similar island growth features are observed on the fivefold surface of i-Al–Pd–Mn and the tenfold surface of d-Al–Ni–Co [3], suggesting that the particular structure of quasicrystals is not responsible for island growth with magic height. The islands of 'magic heights' are observed generally as a result of the quantum size effect, which arises from the confinement of electrons within the film. It is believed that the Bi/i-Al–Cu–Fe interface acts as a confinement barrier if the energy of the Bi sp electrons, which dominate the valence bands of these metals, lies in the pseudogap of the substrate. However, further investigations are required to confirm this.

Recently, Moras *et al* have proposed another model for the electron confinement on the basis of the electronic band structure observation of an Ag thin film deposited on d-Al–Ni–Co and i-Al–Pd–Mn [56]. They argue that the symmetry of wavefunctions is responsible for the confinement.

6. Conclusion

It is found that there are common features among overlayers such as sputter-induced crystalline layers with multiple twin structure on the high symmetry surface of Al-based quasicrystals, the sputter-induced crystalline layer with a single domain on the pseudo-tenfold surface of ξ'-Al–Pd–Mn and crystalline layers with a multiple twin structure induced by surface alloying. These overlayers consist of Al-based alloys with a cubic lattice exposing the $(1\bar{1}0)$-oriented surface. The lattice constant of the cubic lattice is ∼0.3 nm or its integer multiple.

The formation of these overlayers can be understood by means of a simple principle: lattice matching at the interface between overlayers and substrates. These crystalline overlayers appear if an alloy with a lattice constant suited to the quasicrystal surface can be induced by ion sputtering or surface alloying. In the case of quasiperiodic surfaces, the induced overlayer has a multiple twin structure, regardless of ion sputtering and surface alloying. If the substrate has a periodic structure, the overlayer will take the form of a single-domain crystalline layer.

Acknowledgments

This work was partly supported by Solution-Oriented Research for Science and Technology of the Japan Science and Technology Corporation and partly by Grants-in-Aid for Scientific Research from the Ministry of Education, Culture, Sports, Science and Technology, Japan.

References

[1] Fournée V and Thiel P A 2005 *J. Phys. D: Appl. Phys.* **38** R83–106
[2] McGrath R, Ledieu J, Cox E J and Diehl R D 2002 *J. Phys.: Condens. Matter* **14** R119–44
[3] Sharma H R, Shimoda M and Tsai A P 2007 *Adv. Phys.* **56** 403–64
[4] Thiel P A 2004 *Prog. Surf. Sci.* **75** 69–86
[5] Jenks C J, Burnett J W, Delaney D W, Lograsso T A and Thiel P A 2000 *Appl. Surf. Sci.* **157** 23–8
[6] Shimoda M 2004 *Prog. Surf. Sci.* **75** 87–108
[7] Bolliger B, Erbudak M, Hensch A and Vvedensky D D 2000 *Mater. Sci. Eng.* A **294** 859–62
[8] Ledieu J, Munz A W, Parker T M, McGrath R, Diehl R D, Delaney D W and Lograsso T A 1999 *Surf. Sci.* **435** 666–71
[9] Naumović D, Aebi P, Schlapbach L and Beeli C 2000 *Mater. Sci. Eng.* A **294** 882–5
[10] Naumović D, Aebi P, Schlapbach L, Beeli C, Kunze K, Lograsso T A and Delaney D W 2001 *Phys. Rev. Lett.* **87** 195506
[11] Naumović D, Aebi P, Schlapbach L, Beeli C, Lograsso T A and Delaney D W 1999 *Phys. Rev.* B **60** R16330
[12] Noakes T C Q, Bailey P, McConville C F, Parkinson C R, Draxler M, Smerdon J, Ledieu J, McGrath R, Ross A R and Lograsso T A 2005 *Surf. Sci.* **583** 139–50
[13] Shen Z, Kramer M J, Jenks C J, Goldman A I, Lograsso T, Delaney D, Heinzig M, Raberg W and Thiel P A 1998 *Phys. Rev.* B **58** 9961
[14] Shi F, Shen Z, Delaney D W, Goldman A I, Jenks C J, Kramer M J, Lograsso T, Thiel P A and Van Hove M A 1998 *Surf. Sci.* **411** 86–98
[15] Shimoda M, Guo J Q, Sato T J and Tsai A P 2000 *Surf. Sci.* **454** 11–5
[16] Zurkirch M, Bolliger B, Erbudak M and Kortan A R 1998 *Phys. Rev.* B **58** 14113–6

[17] Singh A and Tsai A P 2008 *J. Phys.: Condens. Matter* **20** 314002
[18] Sato T J, Hirano T and Tsai A P 1998 *J. Cryst. Growth* **191** 545–52
[19] Jenks C J, Pinhero P J, Shen Z, Lograsso T A, Delaney D W, Bloomer T E, Chang S L, Zhang C M, Anderegg J W, Islam A H M Z, Goldman A I and Thiel P A 1998 *Proc. 6th Int. Conf. Quasicryst.* p 741
[20] Guo J Q, Hasegawa H, Tsai A P and Takeuchi S 2002 *J. Cryst. Growth* **236** 477–81
[21] Ohhashi S, Hasegawa J, Takeuchi S and Tsai A P 2007 *Phil. Mag.* **87** 3089–94
[22] Fournée V, Ross A R, Lograsso T A, Anderegg J W, Dong C, Kramer M, Fisher I R, Canfield P C and Thiel P A 2002 *Phys. Rev.* B **66** 165423
[23] Eisenmenger-Sittner C, Bangert H, Stöi H, Brenner J and Barn P B 2001 *Surf. Sci.* **489** 161–8
[24] Qin Y L, Wang R H, Wang Q L, Zhang Y M and Pan C X 1995 *Phil. Mag. Lett.* **71** 83–90
[25] Zhang H and Urban K 1992 *Phil. Mag. Lett.* **66** 209–15
[26] Zhang Z, Feng Y C, Williams D B and Kuo K H 1993 *Phil. Mag.* B **67** 237–51
[27] Ferralis N, Pussi K, Cox E J, Gierer M, Ledieu J, Fisher I R, Jenks C J, Lindroos M, McGrath R and Diehl R D 2004 *Phys. Rev.* B **69** 153404
[28] Sharma H R, Franke K J, Theis W, Riemann A, Fölsch S, Gille P and Rieder K H 2004 *Phys. Rev.* B **70** 235409
[29] Kishida M, Kamimura Y, Tamura R, Edagawa K, Takeuchi S, Sato T, Yokoyama Y, Guo J Q and Tsai A P 2002 *Phys. Rev.* B **65** 094208
[30] Suzuki T, Sharma H R, Nishimura T, Shimoda M, Yamauchi Y and Tsai A P 2005 *Phys. Rev.* B **72** 115427
[31] Yuhara J, Klikovits J, Schmid M, Varga P, Yokoyama Y, Shishido T and Soda K 2004 *Phys. Rev.* B **70** 024203
[32] Barrow J A, Fournée V, Ross A R, Thiel P A, Shimoda M and Tsai A P 2003 *Surf. Sci.* **539** 54–62
[33] Shimoda M, Sharma H R and Tsai A P 2005 *Surf. Sci.* **598** 88–95
[34] Boudard M, Klein H, deBoissieu M, Audier M and Vincent H 1996 *Phil. Mag.* A **74** 939–56
[35] Sharma H R, Shimoda M, Fournée V, Ross A R, Lograsso T A and Tsai A P 2005 *Phys. Rev.* B **71** 224201
[36] Tsai A P, Guo J Q, Abe E, Takakura H and Sato T J 2000 *Nature* **408** 537–8
[37] Sharma H R, Shimoda M, Ohhashi S and Tsai A P 2007 *Phil. Mag.* **87** 2989–94
[38] Shimoda M, Guo J Q, Sato T J and Tsai A P 2001 *Surf. Sci.* **482** 784–8
[39] Vitos L, Ruban A V, Skriver H L and Kollár J 1998 *Surf. Sci.* **411** 186–202
[40] Shimoda M, Sato T J, Tsai A P and Guo J Q 2002 *Surf. Sci.* **507** 276–80
[41] Shimoda M, Sato T J, Tsai A P and Guo J Q 2002 *J. Alloys Compounds* **342** 441–4
[42] Shimoda M, Guo J Q, Sato T J and Tsai A P 2004 *J. Non-Cryst. Solids* **334** 505–8
[43] Fournée V, Sharma H R, Shimoda M, Tsai A P, Unal B, Ross A R, Lograsso T A and Thiel P A 2005 *Phys. Rev. Lett.* **95** 155504
[44] Villars P and Calvert L D 1991 *Pearson's Handbook of Crystallographic Data for Intermetallic Phases* vol 1 (Materials Park, OH: ASM International)
[45] Audier M, Durandcharre M and Deboissieu M 1993 *Phil. Mag.* B **68** 607–18
[46] Bolliger B, Erbudak M, Vvedensky D D, Zurkirch M and Kortan A R 1998 *Phys. Rev. Lett.* **80** 5369
[47] Franke K J, Gille P, Rieder K H and Theis W 2007 *Phys. Rev. Lett.* **99** 036103
[48] Widjaja E J and Marks L D 2003 *Phys. Rev.* B **68** 134211
[49] Widjaja E J and Marks L D 2003 *Phil. Mag. Lett.* **83** 47–55
[50] Widjaja E J and Marks L D 2008 *J. Phys.: Condens. Matter* **20** 314003
[51] Theis W 2008 *J. Phys.: Condens. Matter* **20** 314004
[52] van der Vegt H A, Alvarez J, Torrelles X, Ferrer S and Vlieg E 1995 *Phys. Rev.* B **52** 17443
[53] Sharma H R, Shimoda M, Ross A R, Lograsso T A and Tsai A P 2005 *Phys. Rev.* B **72** 045428
[54] Sharma H R, Shimoda M, Ross A R, LoGrasso T A and Tsai A P 2006 *Phil. Mag.* **86** 807–12
[55] Franke K J, Sharma H R, Theis W, Gille P, Ebert P and Rieder K H 2002 *Phys. Rev. Lett.* **89** 156104
[56] Moras P, Weisskopf Y, Longchamp J N, Erbudak M, Zhou P H, Ferrari L and Carbone C 2006 *Phys. Rev.* B **74** 121405